



HAL
open science

Decline of soil respiration in northeastern Tibet through the transition into the Oligocene icehouse

Alexis Licht, Guillaume Dupont-Nivet, N. Meijer, J. Caves-Rugenstein, A. Schauer, J. Fiebig, A. Mulch, C. Hoorn, N. Barbolini, Z. Guo

► To cite this version:

Alexis Licht, Guillaume Dupont-Nivet, N. Meijer, J. Caves-Rugenstein, A. Schauer, et al.. Decline of soil respiration in northeastern Tibet through the transition into the Oligocene icehouse. *Palaeogeography, Palaeoclimatology, Palaeoecology*, 2020, 560, pp.110016. 10.1016/j.palaeo.2020.110016 . insu-02940052

HAL Id: insu-02940052

<https://insu.hal.science/insu-02940052>

Submitted on 16 Sep 2020

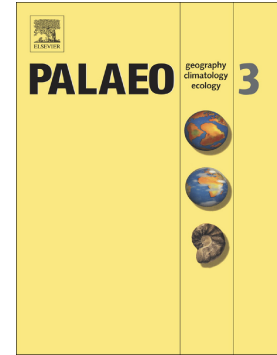
HAL is a multi-disciplinary open access archive for the deposit and dissemination of scientific research documents, whether they are published or not. The documents may come from teaching and research institutions in France or abroad, or from public or private research centers.

L'archive ouverte pluridisciplinaire **HAL**, est destinée au dépôt et à la diffusion de documents scientifiques de niveau recherche, publiés ou non, émanant des établissements d'enseignement et de recherche français ou étrangers, des laboratoires publics ou privés.

Journal Pre-proof

Decline of soil respiration in northeastern Tibet through the transition into the Oligocene icehouse

A. Licht, G. Dupont-Nivet, N. Meijer, J. Caves-Rugenstein, A. Schauer, J. Fiebig, A. Mulch, C. Hoorn, N. Barbolini, Z. Guo



PII: S0031-0182(20)30461-2

DOI: <https://doi.org/10.1016/j.palaeo.2020.110016>

Reference: PALAEO 110016

To appear in: *Palaeogeography, Palaeoclimatology, Palaeoecology*

Received date: 10 April 2020

Revised date: 28 August 2020

Accepted date: 5 September 2020

Please cite this article as: A. Licht, G. Dupont-Nivet, N. Meijer, et al., Decline of soil respiration in northeastern Tibet through the transition into the Oligocene icehouse, *Palaeogeography, Palaeoclimatology, Palaeoecology* (2020), <https://doi.org/10.1016/j.palaeo.2020.110016>

This is a PDF file of an article that has undergone enhancements after acceptance, such as the addition of a cover page and metadata, and formatting for readability, but it is not yet the definitive version of record. This version will undergo additional copyediting, typesetting and review before it is published in its final form, but we are providing this version to give early visibility of the article. Please note that, during the production process, errors may be discovered which could affect the content, and all legal disclaimers that apply to the journal pertain.

© 2020 Published by Elsevier.

Decline of soil respiration in northeastern Tibet through the transition into the Oligocene icehouse

A. Licht^{1,*} licht@uw.edu, G. Dupont-Nivet^{2,3,4} guillaume.dupont-nivet@univ-rennes1.fr, N. Meijer² meijer@uni-potsdam.de, J. Caves-Rugenstein^{5,6} jeremy.caves@gmail.com, A. Schauer¹ aschauer@u.washington.edu, J. Fiebig⁷ Jens.Fiebig@em.uni-frankfurt.de, A. Mulch^{6,7} Andreas.Mulch@senckenberg.de, C. Hoorn⁸ M.C.Hoorn@uva.nl, N. Barbolini^{8,9} barbolini.natasha@gmail.com and Z. Guo⁴ zjguo@pku.edu.cn.

¹Department of Earth and Space Sciences, University of Washington, Seattle, WA USA

²Universität Potsdam, Institute of Geosciences, 14476 Potsdam

³Géosciences Rennes, UMR CNRS 6118, Université de Rennes, 74205 France

⁴Key Laboratory of Orogenic Belts and Crustal Evolution, Peking University, Beijing, 100871 China

⁵Max Planck Institute for Meteorology, Bundesstraße 53, 21460 Hamburg, Germany

⁶Senckenberg Biodiversity and Climate Research Centre, 60325 Frankfurt am Main, Germany

⁷Institute of Geosciences, Goethe University, 60438 Frankfurt am Main, Germany

⁸Department of Ecosystem and Landscape Dynamics, Institute for Biodiversity and Ecosystem Dynamics, University of Amsterdam, 1098 XH The Netherlands

⁹Department of Ecology, Environment and Plant Sciences and Bolin Centre for Climate Research, Stockholm University, SE-106 91 Sweden

* corresponding author.

Abstract: Soil respiration (R_s), the production of carbon dioxide in soils, increases dramatically from deserts to forested ecosystems. R_s values thus provide a potential tool to identify past

ecosystems if recorded in sedimentary archives. Here, we propose a quantitative method to reconstruct past R_s values from paleosols. This method reverses the soil paleobarometer, a proxy that estimates past atmospheric CO_2 concentration values ($\text{CO}_{2\text{atm}}$) from paleosols while considering a narrow range of variation for R_s . We use past $\text{CO}_{2\text{atm}}$ values from marine proxies to reconstruct soil respiration from a 20 million year-long isotopic record from northeastern Tibet covering the transition from the Eocene greenhouse to the Oligocene icehouse. We show that R_s dropped at least 4-fold through the transition into the Oligocene icehouse, marking the spread of boreal desert-steppes of Central Asia. We show that increasing aridity and the decline of monsoonal rainfall, in parallel with global cooling, caused the fall of soil respiration. These highly dynamic R_s emphasize the need for a systematic screening of paleosol isotopic data before using the soil paleobarometer to reconstruct $\text{CO}_{2\text{atm}}$.

Keywords: paleosol, paleoclimate, desertification, Paleogene, atmospheric CO_2 , monsoons

Main Text:

1. Introduction

Soil respiration (R_s , flux, in $\text{gC/m}^2/\text{yr}$) is the carbon dioxide emission from soil microbial activity and plant respiration through the soil surface, exceeds all other terrestrial-atmospheric carbon exchanges with the exception of gross primary productivity (Raich and Potter, 1995). Global fluxes of R_s are estimated around ~ 90 PgC/year (Zhao et al., 2017), roughly nine times more than anthropogenic emissions (Carey et al., 2016), and have increased by ~ 0.05 PgC/year over the last five decades in response to rising temperatures (Jian et al., 2018). Its global dynamics are yet not well understood and it is unclear if and by how much R_s will keep increasing (Bond-Lamberty and Thomson, 2010). The uncertainty in how the global flux of R_s will respond to climate change is due in part to a high variability in R_s values within modern ecosystems (Bond-Lamberty and Thomson, 2010). In forests, R_s values are particularly high (commonly > 900 $\text{gC/m}^2/\text{yr}$) whereas they are very low in deserts and boreal steppes (< 300 $\text{gC/m}^2/\text{yr}$; Table 1; Bond-Lamberty and Thomson, 2018). The high amplitude of R_s values with modern ecosystems has yet a positive side: it provides a discriminatory tool to the evolution of ecosystems for one who can reconstruct past R_s values in sedimentary archives. With the exception of a few recent studies providing low-resolution, first-order estimates of R_s values, for example for the

Carboniferous of Argentina (Gulbranson et al., 2011), the Jurassic of North America (Myers et al., 2012) or the Cenozoic of Asia (Caves-Rugenstein et al., 2018), there have been few attempts to quantify R_s values in deeper time.

Soil CO_2 —the CO_2 in the gas-filled soil pore spaces—is a mixture of atmospheric CO_2 ($\text{CO}_{2\text{atm}}$, concentration in ppmV) that diffuses through the soil and CO_2 produced at depth within the soil from respiration by organisms (S , concentration in ppmV). Mixing of atmospheric and respired CO_2 in well-drained soils yields a simple isotope mass balance relationship (Cerling, 1991; 1999) that links $\text{CO}_{2\text{atm}}$, S , the carbon isotopic composition of soil CO_2 ($\delta^{13}\text{C}_{\text{soil}}$ recorded in soil carbonates), respired CO_2 ($\delta^{13}\text{C}_{\text{resp}}$ recorded in soil organic matter), and atmospheric CO_2 ($\delta^{13}\text{C}_{\text{atm}}$, recorded in marine carbonates). Paleoclimatologists have used this relationship over the last three decades to reconstruct past $\text{CO}_{2\text{atm}}$ from ancient soils by measuring or estimating these three carbon isotopic compositions while making assumptions about past values of S , an approach commonly called “soil paleobarometry” (Cerling, 1999; Ekart et al., 1999; Breecker et al., 2010). Others have used this relationship to reconstruct S by making assumptions about past values of $\text{CO}_{2\text{atm}}$ (Myers et al., 2016; Looy et al., 2016).

There are unfortunately few direct measurements or estimates of S in modern soils (Breecker et al., 2010; Montanez, 2013) and variations of S between and within modern ecosystems is poorly constrained. Montanez (2013) illustrated how S is variable between soil types; within soils of the same type, parameters like soil productivity, soil water saturation, plant growth season timing and duration are expected to influence S . However, S can be linked to soil respiration R_s by making simple assumptions about how CO_2 diffuses in soils (Cerling, 1999; Bowen and Beerling, 2004; Caves et al., 2016). This approach has the advantage of allowing us to compare estimated R_s values with a broad database of modern soil respiration values in different ecosystems for paleoenvironmental interpretations (Table 1). Instead of applying this isotope mass balance relationship to reconstruct past $\text{CO}_{2\text{atm}}$ or S , we here modify the paleobarometry approach to reconstruct past values of R_s , using soil-independent estimates of past $\text{CO}_{2\text{atm}}$ (Caves-Rugenstein et al., 2018). We then apply this approach to several well-dated soil sequences in the Xining Basin, in northeastern Tibet (Fig. 1), in order to quantitatively reconstruct the evolution of soil respiration covering the late Paleogene Greenhouse to Icehouse transition, a period of declining $\text{CO}_{2\text{atm}}$ (Fig. 2a).

2. Method to reconstruct soil respiration rates

2.1 Principles

Reconstructing soil respiration rates from carbon isotopic data and $\text{CO}_{2\text{atm}}$ values requires the use of three equations. First, mixing of atmospheric and respired CO_2 in soil follows the soil barometry equation first proposed by Cerling (1984), derived from an isotope mass balance relationship at soil depth z :

$$S(z) / \text{CO}_{2\text{atm}} = (\delta^{13}\text{C}_{\text{atm}} - \delta^{13}\text{C}_{\text{soil}}) / (\delta^{13}\text{C}_{\text{soil}} - 1.0044 \delta^{13}\text{C}_{\text{resp}} - 4.4) \quad (1)$$

This equation links $\text{CO}_{2\text{atm}}$ to $\delta^{13}\text{C}_{\text{soil}}$, $\delta^{13}\text{C}_{\text{atm}}$, $\delta^{13}\text{C}_{\text{resp}}$ and $S(z)$, which is S (in ppmV) at soil depth z . Note that $\delta^{13}\text{C}_{\text{resp}}$ is recorded in soil organic matter and is thus directly recoverable (Breecker, 2013); paleo- $\delta^{13}\text{C}_{\text{atm}}$ has been reconstructed in deep time from marine carbonates (Tippie et al., 2010).

$S(z)$ is a function of the soil CO_2 production rate at the surface Φ_s (in mole/cm³/s) following the equation of Cerling and Quade (1993) for the evolution of $S(z)$ through soil profile:

$$S(z) = (\Phi_s z_c^2 / (D_s \varepsilon)) (1 - \exp(-z/z_c)) \quad (2)$$

This equation links $S(z)$ (here in mole/cm³), Φ_s and various soil parameters including the diffusional constant for CO_2 D_s (in cm²/s), free-air soil porosity ε (dimensionless quantity; Bowen and Beerling, 2004; Caves et al., 2016), and the characteristic depth of CO_2 production in soils z_c (in cm). When integrated over total soil depth z_p (in cm), this equation becomes:

$$R_s = \Phi_s z_c - \Phi_s z_c \exp(-z_p / z_c) \quad (3)$$

The carbon isotopic composition of soil CO_2 ($\delta^{13}\text{C}_{\text{soil}}$) can be retrieved from soil carbonates. Pedogenic carbonate commonly forms in equilibrium with soil CO_2 ; its carbon isotopic composition ($\delta^{13}\text{C}_{\text{carb}}$) is directly linked to the isotopic composition of soil CO_2 , with a fractionation factor depending on soil temperature T (Romanek et al., 1992):

$$\alpha_{\text{carb-soil}} = 11.98 - 0.12 T \text{ where } \alpha_{\text{carb-soil}} = 1000 [(\delta^{13}\text{C}_{\text{carb}} + 1000) / (\delta^{13}\text{C}_{\text{soil}} + 1000) - 1] \quad (4)$$

Our method relies on a simple procedure. From measured $\delta^{13}\text{C}_{\text{carb}}$ and T at soil sampling depth z_s (in cm), we determine $\delta^{13}\text{C}_{\text{soil}}$ with equation (4). With $\delta^{13}\text{C}_{\text{soil}}$ and $\delta^{13}\text{C}_{\text{resp}}$ measured from soil organic matter, $S(z_s)$ is calculated in ppmV with equation (1), assuming $\text{CO}_{2\text{atm}}$ and $\delta^{13}\text{C}_{\text{atm}}$ from independent studies (see below). $S(z_s)$ is converted in mole/cm³ using the ideal gas law at temperature T , and used to calculate Φ_s from equation (2) at depth z_s . R_s is calculated from Φ_s and equation (3), both equations using a modern-like range of soil parameters D_s , ε , z_p , and z_c values (Table 2). The sensitivity of this approach to model parameters is investigated in Caves et al. (2016). Among all parameters, $\text{CO}_{2\text{atm}}$ is the one with the most important impact on reconstructed R_s values.

For our model, the diffusional constant for CO_2 was given a single value of $D_s=0.042$ cm²/s; similarly, soil porosity was given a single value $\varepsilon=0.6$. These values correspond to averaged values in modern soils (Cerling and Quade, 1993; Caves et al., 2016) and are used as constant.

To take into account the uncertainty in soil characteristic depth z_c and soil profile depth z_p , as well as in soil sampling depth z_s (which is often not reported or hard to determine for paleosols because soil horizons are sometime lacking), these three parameters were given a random uniformly-distributed error around a pre-determined value: $z_p=100 \pm 20$ cm. $z_c = 25 \pm 10$ cm, $z_s=50 \pm 10$ cm. For z_p and z_c , these values correspond to average values and observed variations in modern non tropical well-drained soils (Cerling and Quade, 1993; Caves et al., 2016); z_s values correspond to the common depth of calcareous horizons in soils and the usual sampling depth in paleo-studies (Cerling, 1992; Kretzschmar, 2005; Caves et al., 2016). We performed a Monte Carlo approach: for 20000 simulations, we randomly picked the value of these three parameters within their error interval and calculated R_s every time. We then produced a mean (average) R_s value and its standard deviation over the 20000 simulations.

2.2 Validation

We applied this approach to modern soils, with modern $\text{CO}_{2\text{atm}}$ and $\delta^{13}\text{C}_{\text{atm}}$ to test how accurately this model can predict modern soil respiration values. Values for soil $\delta^{13}\text{C}_{\text{carb}}$ and $\delta^{13}\text{C}_{\text{resp}}$ in different biomes were taken from three studies (Cerling, 1992; Cerling and Quade, 1993; Ekart et al., 1999); maximum temperature at 50 cm soil depth, when available, or growth season temperature + 5°C (following Breecker et al., 2009) were used as carbonate growth temperature T . Our method successfully reproduced average soil respiration for most biomes as

well as soil respiration from nearby sites (Caldwell et al., 1977; De Jong, 1981; Fouseki et al., 1981; Wang et al., 1993; Hudgens and Yavitt, 1997; Knapp et al., 1998; Craine et al., 1999; Tüfekçioğlu et al., 2010; Table 3). Only soils from temperate grasslands of North America exhibit lower-than-expected R_s values; we attribute this misfit to the fact that the temperate grasslands of North America have experienced significant Holocene ecosystem restructuring with a change in the component of C_4 plants. This created temporal misfits between $\delta^{13}C_{carb}$ and $\delta^{13}C_{resp}$ as soil carbonates grow over long period of times (several kyr) and therefore time-average longer periods compared to organic matter (Wang et al., 1993). However, this source of discrepancies should not impact our Paleogene data derived from before the spread of C_4 plants in the Neogene.

2.3 Limitations

Our model has several important limitations that need to be acknowledged before any interpretation of reconstructed R_s values.

Soil carbonates only form when the ground dries and soil respiration decreases after seasonal rainfall; this phenomenon is favored during warmer seasons because high soil temperatures decrease calcite solubility, and evaporation and plant evapotranspiration increase calcium activity in the soil water (Breecker et al., 2009). In most areas, including in our study area, Tibet, carbonate growth occurs mostly during the summer (Quade et al., 2013); it is unclear if carbonate growth occurs before monsoonal rainfall in June (Quade et al., 2013) or during soil dewatering after individual monsoonal storms (Hough et al., 2014). Therefore, an alternative way to think about the respiration rates reconstructed here is that they represent minimum summer season respiration rates.

The direct implication of this seasonal bias is that reconstructed R_s by our approach might overestimate annual respiration rates. There are unfortunately very few available measurements of summer season respiration rates in the world-wide Soil Respiration Database (often <10 measurements per ecosystem world-wide; Table 1), and minimum summer season respiration rates are virtually undocumented. Summer is synchronous or shortly follows the plant growing season in most places and summer respiration rates should thus be higher than annual rates. This is confirmed by the few measurements available in the Soil Respiration Database, showing summer values 1x to 6x times greater than annual rates. However, as our reconstructed R_s values likely reflect minimum summer soil respiration rates, this over-estimation might be insignificant and is not expressed at the modern test localities discussed in the previous section.

A second limitation when dealing with isotopic datasets including many soil and/or paleosol data is that important factors other than soil respiration may affect reconstructed R_s values. Changes in soil type or soil grain-size in particular (Montanez 2013; Breecker, 2013) would result in artificially varying R_s values as our model includes a limited range of soil parameters (for D_s , ϵ , z_p , and z_c). For a given soil type and grain-size, an increase of soil water saturation would result in a significant decrease of both D_s and ϵ values (Cerling and Quade, 1993); in our model, decreasing D_s and ϵ results in an increase in the reconstructed R_s . This needs to be kept in mind for the following application.

3. Application to Paleogene soils from northeastern Tibet

3.1 Geological context

The 100-km wide Xining Basin lies at the transition between the Asian desert belt and the semi-arid Chinese Loess Plateau—the deserts' dust trap (Fig.1; Licht et al., 2016). The basin attains elevations of ~2000 m but likely stood near sea-level during the late Paleogene, 40 to 23 million years ago (Page et al., 2019). Present-day rainfall is sparse (~350 mm of annual precipitation) and monsoonal, with 70% of precipitation occurring during the summer and the remaining part occurring during the winter from westerly-derived moisture (Page et al., 2019); the contribution of westerly-derived moisture might have been more significant in the Paleogene (Meijer et al., 2019). In contrast to the present-day dominance of boreal steppe vegetation, Eocene vegetation was dominated by desert-steppe shrubs together with temperate deciduous forest taxa, indicating a more temperate landscape of desert-steppe and woodlands (Hoorn et al., 2012); late Eocene sediment also contains conifer pollen blown in from the surrounding highlands (Hoorn et al., 2012; Page et al., 2019). Paleogene sedimentary units are dominated by carbonate-bearing red mudstone deposited on a dry mudflat, partly composed of dust and forming poorly developed aridisols (Licht et al., 2016), with cyclic gypsum deposits formed from the evaporation of playa lakes (Abels et al., 2011; Meijer et al., 2019); gypsum bed thicknesses decrease through the late Eocene and they eventually completely disappear through the EOT, indicating increased aridity (Dupont-Nivet et al., 2007; Abels et al., 2011). There is no change in pedogenic style, paleosol texture or grain-size in the red mudstones through the studied interval (Abels et al., 2011; Licht et al., 2014).

3.2 Stable isotope analysis

We collected 219 samples of carbonate-bearing mudstones from the Xining Basin along three previously dated (and temporally overlapping) sections covering the time interval from the middle Eocene to the earliest Miocene, at the locality of Shuiwan (Abels et al., 2011), Tiefu (Bosboom et al., 2014), and Xieja (Dai et al., 2006). These sections have been dated at high resolution by a combination of magnetostratigraphy and cyclostratigraphy (Dai et al., 2006; Abels et al., 2011; Bosboom et al., 2014; Dupont-Nivet et al., 2007; Fang et al., 2019). The cyclicity of gypsum / red mudstone alternations in the Xining record allows us to date Eocene samples at the resolution of one obliquity cycle (41 kyr). Oligocene samples are dated by magnetostratigraphy only, due to the lack of clear cyclicity in the Oligocene part of the Xining record; we estimate the uncertainty around the age of our Oligocene samples to be ~80-100 kyr based on accumulation rate variation (Dai et al., 2006). Test samples were prepared in thin section and examined using cathodoluminescence and polarized light microscopy to evaluate the origin and potential for diagenesis of the carbonates (Page et al., 2019). Carbonates were identified as vadose-grown, pedogenic cements and did not show any evidence for subsequent diagenetic alteration. Pedogenic vadose-grown cements precipitate from soil water and commonly display the same oxygen and carbon isotope values and growth season as pedogenic nodules (Quade and Roe, 1999; Fan et al., 2018). Our diagenetic screening and identification of the origin of the Xining carbonates is thoroughly discussed in a previous publication (Page et al., 2019).

Half of every sample was decarbonated with 6N HCl twice and washed with 18 M-ohm water several times for acid removal; Carbon content and organic matter $\delta^{13}\text{C}$ values were then measured with a Costech elemental analyzer coupled to a Thermo MAT253 gas source isotope ratio mass spectrometer (University of Washington) or with a Flash Elemental Analyzer 1112 connected to a Thermo MAT253 gas source isotope ratio mass spectrometer (Goethe University-Senckenberg BiK-F Stable Isotope Facility, Frankfurt). Measured carbon isotopic compositions were corrected using in-house reference materials. International reference materials USGS 24 and IAEA-CH-7 were analyzed along with the samples to check for accuracy. The other half of every sample was reacted with 105 % orthophosphoric acid; carbonate $\delta^{18}\text{O}$ and $\delta^{13}\text{C}$ values were measured with a Kiel III Carbonate Device coupled to a Thermo Finnigan Delta Plus gas source isotope ratio mass spectrometer (University of Washington) or with Thermo GasBench II interfaced with a Thermo MAT 253 gas source isotope ratio mass spectrometer (Goethe

University-Senckenberg BiK-F Stable Isotope Facility, Frankfurt). Measured carbon content, carbon and oxygen isotopic compositions were corrected using in-house reference materials as well as NBS18 and NBS19 carbonate reference materials. All $\delta^{13}\text{C}$ and $\delta^{18}\text{O}$ values are expressed relative to VPDB. All data are available in Supplementary Data S1.

3.3 Reconstruction of soil respiration rates

For our Paleogene samples, we modified the Monte Carlo approach to take into account additional uncertainties in sample ages, carbonate growth temperature, and past $\text{CO}_{2\text{atm}}$ and $\delta^{13}\text{C}_{\text{atm}}$ values.

The age uncertainty was considered to be ± 80 kyr for all samples, corresponding to ~ 2 obliquity cycles. Carbonate growth temperatures were calculated from clumped isotopic values from a subset of 20 samples of the same dataset, already published in Page et al. (2019): temperatures were attributed to each additional sample in the dataset by calculating a moving average across the available clumped isotope temperatures (rolling windows: 2.4 Myr); uncertainties correspond to the maximum standard error observed over the time window (between 4 to 7°C; Fig. 2b). $\delta^{13}\text{C}_{\text{carb}}$ and $\delta^{13}\text{C}_{\text{resp}}$ are from red mudstone carbonates (Fig. 2c) and organic matter (Fig. 2d).

We used two different $\text{CO}_{2\text{atm}}$ scenarios for past $\text{CO}_{2\text{atm}}$ values. Our first $\text{CO}_{2\text{atm}}$ scenario is based on a moving average across a late Paleogene $\text{CO}_{2\text{atm}}$ database, excluding data based on soil paleobarometry. $\text{CO}_{2\text{atm}}$ values are taken from a rolling window (width: 4 Myr) across a cleaned database of existing $\text{CO}_{2\text{atm}}$ values downloaded from Gavin Foster's website (Foster, 2019) of marine proxies (boron; Anagnostou et al., 2016; and alkenones; Pagani et al., 2011) to which we added leaf stomata proxies (Steinhilber et al., 2016); all data and references are in Supplementary Data S2, as well as the final T and $\text{CO}_{2\text{atm}}$ age models used here. $\text{CO}_{2\text{atm}}$ values are randomly picked within the quartiles Q1 and Q3 in the time window (Fig. 2a). We alternatively used a synthetic one-step scenario with a sudden twofold decrease of $\text{CO}_{2\text{atm}}$ at 33.9 Ma (Fig. 2a): 800 ± 200 ppmV before 33.9 Ma, 400 ± 200 ppmV after 33.9 Ma. This scenario corresponds to scenarios used to explain the onset of ice-sheet expansion at the Eocene-Oligocene Transition (Licht et al., 2014) (EOT), and is identified in several individual marine records (Pagani et al., 2011). Note that rolling windows for the moving averages for T and $\text{CO}_{2\text{atm}}$ are particularly large due to the lack of carbonate growth temperature or $\text{CO}_{2\text{atm}}$ data during some intervals of the Paleogene. Finally, $\delta^{13}\text{C}_{\text{atm}}$ is randomly picked at -6 ± 0.25 ‰, corresponding to the atmospheric

CO₂ carbon isotopic composition of the 40-20 Ma time window (Tippie et al., 2010). Diffusional constant for CO₂ D_s and soil porosity ϵ were used as constant as no change of grain-size or pedogenic style is observed in the sampled sections.

Allowing the Monte Carlo approach to cover a wide range of T can in a few cases result in incompatible ($\delta^{13}\text{C}_{\text{soil}}$, $\delta^{13}\text{C}_{\text{resp}}$) pair values, leading to unrealistic, anomalously high or negative S(z) values from equation (1) for which the fractionation rule between soil-respired and soil carbon (Cerling, 1999) $\delta^{13}\text{C}_{\text{soil}} - 1.0044 \delta^{13}\text{C}_{\text{resp}} - 4.4 \gg 0$ is not respected. To avoid these inconsistencies, our Monte Carlo procedure rejects any soil temperature T that results in $\delta^{13}\text{C}_{\text{soil}} - 1.0044 \delta^{13}\text{C}_{\text{resp}} - 4.4 < 0.5$; this threshold results in only realistic R_s values ($R_s < 10\,000$ gC/m²/yr). This procedure rejects 1 to 4% of the randomly picked T.

We finally performed the same Monte Carlo approach as for the modern samples: for 20000 simulations, we randomly picked the value of the six parameters within their error interval (z_p , z_c , z_s , age, T, CO_{2atm}) for each of the 219 data points, and calculated S(z) and R_s for every data point. A temporal moving average (rolling window: 0.5 Myr) and its standard deviation are then calculated over all the 20000 simulations (Fig. 2e and 2f). The Matlab code used to compute the soil respiration for modern and Paleogene data is provided in the supplementary material.

3.4 Calculation of soil water $\delta^{18}\text{O}$

In addition to respiration rates, we plotted Xining pollen assemblages (Fig. 2g; Page et al., 2019) and the measured carbon content in our samples (Fig 2h). We also reconstructed soil water $\delta^{18}\text{O}$ values from carbonate $\delta^{18}\text{O}$ values as a proxy for rainfall isotopic composition, that can be regionally linked to climatic parameters (Licht et al., 2014; Caves et al., 2016). Soil water $\delta^{18}\text{O}$ was calculated from carbonate $\delta^{18}\text{O}$ values using the standard calcite-water fractionation equation (Kim and O'Neil, 1997) linking soil water $\delta^{18}\text{O}$, carbonate $\delta^{18}\text{O}$ and carbonate growth temperature. For each carbonate sample, the temperature and associated temperature uncertainty were attributed from clumped isotope-based temperature, the same way as for the calculation of R_s (Fig. 2b). For 20000 simulations, we randomly picked the value of carbonate growth within its error interval for each of the 219 data points, and calculated soil water $\delta^{18}\text{O}$ for every data point. A temporal moving average (rolling window: 0.5 Myr) and its standard deviation are then calculated over all the 20000 simulations (Fig. 2i). The resulting standard deviation per soil water $\delta^{18}\text{O}$ is in average 0.6 ‰, and always lower than 0.9 ‰.

Soil water $\delta^{18}\text{O}$ values for Xining are then compared with modern rainfall $\delta^{18}\text{O}$ values from Lanzhou, GNIP station located 200 km away from Xining (Araguas-Araguas et al., 1998; Hough et al., 2011). Lanzhou is at lower elevation than the modern-day Xining Basin, making it a better comparison location for the Paleogene; Lanzhou today receives more late spring and summer rainfall (85 % of total annual rainfall) than Xining. Both the difference in elevation and in monsoonal rainfall contribution make modern Xining rainfall $\delta^{18}\text{O}$ \sim 1-2 ‰ lower in average than Lanzhou rainfall (Zhang et al., 2002).

All our code is now available in the supplementary material as Matlab files.

4. Results

For both $\text{CO}_{2\text{atm}}$ scenarios, reconstructed Eocene $S(z)$ are high: 4044 ± 1350 (1 σ) ppmV for the data-based $\text{CO}_{2\text{atm}}$ scenario, 3869 ± 1276 (1 σ) ppmV for the synthetic $\text{CO}_{2\text{atm}}$ scenario on average during the 39 to 35.5 Ma period. These scenarios result in high R_s values, in the range of annual soil respiration found in well-drained soils of temperate grasslands and woodlands (Fig. 2f): 758 ± 256 (1 σ) $\text{gC/m}^2/\text{yr}$ for the data-based $\text{CO}_{2\text{atm}}$ scenario, 725 ± 242 (1 σ) $\text{gC/m}^2/\text{yr}$ for the synthetic $\text{CO}_{2\text{atm}}$ scenario. These R_s values are in agreement with a temperate landscape of desert-steppe and woodlands as seen in pollen data (Horn et al., 2012).

During a short interval in the Eocene, between 37.5 and 36 Ma, $S(z)$ values peak up to \sim 7500 ppmV while R_s values reach \sim 1300 $\text{gC/m}^2/\text{yr}$, higher than annual soil respiration found today in most temperate ecosystems. Considering that there is no change of pedogenic style or grain-size during this interval, we narrow the potential mechanisms responsible for this excursion down to three non-exclusive scenarios. First, these values could potentially reflect increased summer-bias in the soil respiration record, driving reconstructed $S(z)$ and R_s values above annual averages. They could also indicate soil water saturation, thereby limiting CO_2 diffusion in the soil and biasing R_s values towards high values. Finally, they could also reflect a short drop of $\text{CO}_{2\text{atm}}$ that would not be recorded in our database and drive reconstructed $S(z)$ and R_s values up.

Reconstructed $S(z)$ and R_s values then drastically decline between 35.5 to 34 Ma, reaching values lower than 1000 ppmV for $S(z)$ (960 ± 103 and 488 ± 57 ppmV for both scenarios respectively) and lower than 200 $\text{gC/m}^2/\text{yr}$ for R_s (179 ± 19 and 91 ± 10 $\text{gC/m}^2/\text{yr}$ for both scenarios respectively) between the EOT and the Oi-1 glaciation at 33.5 Ma. This is recorded in a significant increase in soil carbonate $\delta^{13}\text{C}$ values, increasing by 2-3 ‰ during the latest Eocene

(Fig. 2c). Shortly after the Oi-1 glaciation, soil organic matter $\delta^{13}\text{C}$ values drop by 2-3 ‰ (Fig. 2d) keeping the reconstructed $S(z)$ and R_s low until the end of our record in the latest Oligocene. This drop is associated with a stabilization to low values for the soil carbon content (Fig. 2h).

5. Discussion

5.1 Paleoenvironmental implications

Taken at face value, lower soil organic matter $\delta^{13}\text{C}$ values after the Oi-1 glaciation suggest less water stress on plants and a change to a wetter biome (Kohn, 2010). However, the lower soil carbon content (Fig. 2h) and the disappearance of lacustrine deposits (Dupont-Nivet et al., 2007) rather indicate a change to a more desertic ecosystem. This is corroborated by the decrease in the representation of Eocene steppe floras at the expense of conifer pollen (Fig 2g; Hoorn et al., 2012; Page et al., 2019), as modern desert vegetation areas on the Tibetan Plateau display unusually high amount of conifer pollen carried by winds over long distances (Herzschuh, 2007). A shift from a warm temperate desert-steppe and woodland ecosystem to a similar-to-modern cold boreal desert-steppe could reduce water stress on plants and is more compatible with low respiration rates (cf Table 1).

Importantly, the 4- to 7-fold drop in reconstructed R_s is achieved by the EOT and before the change to colder conditions at the Oi-1 glaciation. The onset of R_s decline is almost synchronous with the appearance of the first conifer pollen in Xining, suggesting that the long-term, gradual decrease of global temperature during the late Eocene could explain part of this decline (Pagani et al., 2011). But the onset of R_s decline precedes most of the temperature decrease during the transition into the Oligocene icehouse, marked by the Oi-1 glaciation (Miller et al., 2009), as reflected in the Xining Basin clumped isotope temperature record (Page et al., 2019). It is thus likely that local temperature changes alone did not significantly affect the drop of reconstructed R_s . The Xining pollen record does not exhibit any fundamental change of ecosystem between 37 and 34 Ma. However, a decrease in vegetation cover and associated loss of soil carbon could have significantly weakened soil respiration. This interpretation is in agreement with the stabilization to low values for the soil carbon content after the EOT (Fig. 2h) and increased aridity shown by the stepwise disappearance of lacustrine beds (Dupont-Nivet et al., 2007; Abels et al., 2011).

An alternative way of interpreting our data is to consider that our proxy only records a snapshot of soil respiration during carbonate growth and that the drop of R_s could be explained by a gradual shift of carbonate formation outside the summer growing season, the monsoonal season in Tibet (Breecker et al., 2010). Eocene carbonate growth temperatures from the clumped isotopic record in Xining display large-magnitude changes that can only be explained by a combination of temperature variations and shifts of carbonate growth between warmer and cooler months (Page et al., 2019). These shifts to cooler months have been interpreted to reflect a decline of monsoonal intensity, increasing the proportion of carbonate growing in spring, when the soils start to dry out after the winter rains (Page et al., 2019). Such a scenario is compatible with our reconstructed R_s , as the drop of R_s could be explained by a long-term shift of carbonate growth to earlier months. The shift to more negative soil organic matter $\delta^{13}\text{C}$ values would thus require an increase in winter westerly-derived moisture to reduce water-stress on plants. However, there is no systematic correlation between carbonate growth temperature (Fig. 2b) and reconstructed R_s during the Eocene part of our record. This suggests that changes of carbonate growth season did not play the only role, and that both ways of interpreting our data are required: a long-term, late Eocene decrease in monsoonal intensity would have reduced vegetation cover (Hoorn et al., 2012) and weakened soil respiration as well as shifted the carbonate growth season to the spring.

Soil water oxygen isotope ratios $\delta^{18}\text{O}$ (Fig. 2i) reconstructed from the Xining carbonates provide insight into regional rainfall patterns. Eocene soil water displays highly dispersed $\delta^{18}\text{O}$ values indicative of a combination of late spring to summer, mostly monsoonal water and winter, westerly-derived water, and/or strong soil evaporative effects that shift soil $\delta^{18}\text{O}$ to higher values (Quade et al., 1989). Average $\delta^{18}\text{O}$ values gradually decrease into the late Eocene and soil water $\delta^{18}\text{O}$ values converge to westerly-derived moisture values in the earliest Oligocene, reflecting an apparent absence of East Asian monsoonal moisture in the soil hydrological budget. These values corroborate both the long-term aridification trend culminating at the EOT (Dupont-Nivet et al., 2007; Abels et al., 2011) and the decrease in East Asian monsoonal intensity (Page et al., 2019), likely responsible for the regional aridification, which would have resulted in a significant dwindling of vegetation cover and weakened soil respiration. This chronology indicates that the first step of the expansion of Central Asian deserts is tightly linked to global cooling and likely poorly related to Tibetan uplift (Liu et al., 2015).

The chronology of desertification in the Xining Basin differs from what is seen in other Tibetan basins. Paleobotanical and sedimentological data suggest the persistence of wet conditions further west in the Qaidam Basin during the Oligocene (Song et al., 2020) and a shift to wetter conditions further south in the Jianshuan Basin ~2 Ma before the EOT (Sorrel et al., 2016). The higher paleoelevation of these two basins likely favored wetter paleoenvironments (Wu et al., 2018; Song et al., 2020); nonetheless, these results indicate that alternate sources of atmospheric moisture to Tibet (westerly winds, South Asian monsoon) remained significant during the Oligocene. In particular, the onset of desertification in the Xining Basin is 10 million years before the appearance of the first ergs in western China (Zheng et al., 2015; Jia et al., 2020), indicating that westerly-derived moisture remained a significant source of humidity further west for millions of years after the EOT (Fig. 1).

5.2 Implications for soil paleobarometry

It has already been recognized that secular changes in soil respiration in paleosols at a given locality can be quite large (e.g. Cotton et al., 2015). Our results confirm these findings and raise doubts about the accuracy of past $\text{CO}_{2\text{atm}}$ data acquired with the soil paleobarometry approach, that uses a narrow range of soil respiration values, either related to the pedogenic style of the paleosol (Montanez, 2013) or to the depth of the calcic horizon, often seen as controlled by rainfall (Retallack, 2009; Cotton and Sheldon, 2012). To illustrate this, we run the method developed here by assuming known soil respiration at $400 \pm 100 \text{ gC/m}^2/\text{yr}$ and calculate the resulting evolution of atmospheric $\text{CO}_{2\text{atm}}$ through our record. This range of soil respiration values correspond to a range for $f(z)$ of $2228 \pm 528 \text{ ppmV}$ in our model, overlapping with values commonly used in other global $\text{CO}_{2\text{atm}}$ reconstructions based upon soil carbonate $\delta^{13}\text{C}$ (2000 to 2500 ppmV; Breecker et al., 2010; Foster et al., 2017); these soil respiration values also overlap with average values used in paleobarometry for arid soils (Montanez, 2013) or for a constant sampling depth of 40 to 60 cm (Retallack, 2009), as found in our record.

Instead of using $\text{CO}_{2\text{atm}}$ as an input, with its values being randomly picked within an error interval, we use instead R_s as an output, with values randomly picked within this $400 \pm 100 \text{ gC/m}^2/\text{yr}$ window. Reconstructed $\text{CO}_{2\text{atm}}$ values increase 2- to 5-fold between the late Eocene and the late Oligocene, contradicting other $\text{CO}_{2\text{atm}}$ and temperature records and the geological record of glaciation across the EOT (Fig. 3). These results highlight that our knowledge of past $\text{CO}_{2\text{atm}}$

variations, often based on soil paleobarometry as an important component of current datasets (Foster et al., 2017), may be significantly biased by large differences in R_s values in deep time.

A potential leverage to avoid such bias would be to select paleosol samples for which soil respired CO_2 at sampling depth $S(z_s)$ and $\text{CO}_{2\text{atm}}$ are “balanced” (in equal concentration), as proposed by Breecker (2013). This can be ensured by selecting paleosols for which equation (1) has a narrow range of values around 1. This approach rejects all our Eocene $\text{CO}_{2\text{atm}}$ reconstructions due to their high respiration rates, but our Oligocene soils would still pass this test while yielding unrealistic values for $\text{CO}_{2\text{atm}}$ (> 2000 ppmV). This overestimation is due to the fact that the soil respiration values commonly used for $\text{CO}_{2\text{atm}}$ reconstructions are too high for our soils, highlighting the need for better independent constraints on past $S(z_s)$. Alternatively, Montanez (2013) showed that many modern soils with moderate to high soil respiration values have a narrow range of $(\delta^{13}\text{C}_{\text{soil}}, \delta^{13}\text{C}_{\text{resp}})$ couplets and proposed to use threshold $(\delta^{13}\text{C}_{\text{carb}}, \delta^{13}\text{C}_{\text{resp}})$ values to screen data for the use of soil paleobarometry. Montanez’s screening criterion ($12.2\% < \delta^{13}\text{C}_{\text{carb}} - \delta^{13}\text{C}_{\text{om}} < 15.8\%$) corresponds to selecting paleosol data for which $S(z_s)$ is 1.5 to 3x the value of $\text{CO}_{2\text{atm}}$ and reject paleosols with low soil respiration. When applied to our dataset, this approach rejects most of our data except for Eocene data of the interval 38–36 Ma, when $S(z)$ values peak above 5000 ppmV. This second approach for screening soil paleobarometry data is more satisfying, as the reconstructed $\text{CO}_{2\text{atm}}$ values for the 38–36 Ma interval, at 693 ± 198 ppmV (1s) on average, appear in good agreement with other $\text{CO}_{2\text{atm}}$ proxies (Fig. 3).

6. Conclusions

Our new approach to reconstruct soil respiration rates, when applied to the Xining paleosol record, reveals highly dynamic soil respiration through time. The location of our study, at the edge of the East Asian monsoonal domain, makes its paleoenvironments particularly sensitive to global climate change and might explain the significant amplitude of R_s variation through our record. The significant drop in vegetation cover interpreted from pollen data, soil respiration rates, and temperature mark the onset of the first cold desert-steppes of central China across the EOT. It confirms a major desertification step in Central Asia through the fall into the Oligocene Icehouse associated with decreasing monsoonal intensity.

Our results also emphasize that the soil paleobarometry approach to reconstruct past $\text{CO}_{2\text{atm}}$ should be used with a careful screening of paleosol isotopic data; changes of soil CO_2 are at least as sensitive to changes of $\text{CO}_{2\text{atm}}$ as to secular changes in environmental factors and soil respiration, which are poorly constrained in the stratigraphic record. Nevertheless, this sensitivity to soil respiration can be leveraged to yield critical constraints on the sensitivity of poorly understood biogeochemical fluxes. Although restricted to mid-latitudes, where pedogenic carbonates form, our new approach opens avenues for a detailed documentation of soil respiration and desert expansions and retreats in deep time (when $\text{CO}_{2\text{atm}}$ is constrained), with important implications for our understanding of past ecosystems and hydrological budgets.

The following are the supplementary data related to this article.

Supplementary data 1

Supplementary data 2

Supplementary material

Acknowledgments: This study was financially supported by The University of Washington. GD-N, NM and NB acknowledge funding from ERC consolidator grant MAGIC 649081. JKCR is funded by a Humboldt post-doctoral fellowship. We thank K. Huntington, M. Kaya and A. Rohrmann for prolific discussions and assistance in the field; we also thank Dan Breecker, Nathan Sheldon, Isabel Montañez and two anonymous referees for their comments during the review process.

Author Contributions: A.L. and G.D.-N. conceived the project. A.L., N.M., and Z.G. collected the samples. A.L., A.S., J.F. and A.M. performed isotopic analyses. A.L., G.D.-N., and J.C.-R. wrote the manuscript with contributions from all authors. Authors declare no competing interests.

Data and materials availability: All data is available in the main text or the supplementary materials.

References:

- Abels, H. A., Dupont-Nivet, G., Xiao, G., Bosboom, R., & Krijgsman, W., 2011, Step-wise change of Asian interior climate preceding the Eocene–Oligocene Transition (EOT). *Palaeogeography, Palaeoclimatology, Palaeoecology*, 299(3), 399-412.
- Anagnostou, E., John, E. H., Edgar, K. M., Foster, G. L., Ridgwell, A., Inglis, G. N., ... & Pearson, P. N. (2016). Changing atmospheric CO₂ concentration was the primary driver of early Cenozoic climate. *Nature*, 533 (7603), 380-384.
- Araguás-Araguás, L., Froehlich, K., & Rozanski, K. (1998). Stable isotope composition of precipitation over southeast Asia. *Journal of Geophysical Research: Atmospheres*, 103(D22), 28721-28742.
- Bond-Lamberty, B., & Thomson, A. (2010). Temperature-associated increases in the global soil respiration record. *Nature*, 464(7288), 579-582.
- Bond-Lamberty, B. P., & Thomson, A. M. (2018). A Global Database of Soil Respiration Data, Version 4.0. ORNL DAAC.
- Bosboom, R.E., Abels, H.A., Hoorn, C., van de Berg, B.C., Guo, Z. and Dupont-Nivet, G., 2014, Aridification in continental Asia after the Middle Eocene Climatic Optimum (MECO). *Earth and Planetary Science Letters*, 389, 34-42.
- Bowen, G. J., & Beerling, D. J. (2014). An integrated model for soil organic carbon and CO₂: Implications for paleosol carbonate CO_{2atm} paleobarometry. *Global Biogeochemical Cycles*, 18(1), GB1026.
- Breecker, D. O., Sharp, Z. D., & McFadden, L. D. (2009), Seasonal bias in the formation and stable isotopic composition of pedogenic carbonate in modern soils from central New Mexico, USA. *Geological Society of America Bulletin*, 121(3-4), 630-640.
- Breecker, D. O., Sharp, Z. D., & McFadden, L. D. (2010). Atmospheric CO₂ concentrations during ancient greenhouse climates were similar to those predicted for AD 2100. *Proceedings of the National Academy of Sciences*, 107(2), 576-580.
- Breecker, D. O. (2013). Quantifying and understanding the uncertainty of atmospheric CO₂ concentrations determined from calcic paleosols. *Geochemistry, Geophysics, Geosystems*, 14(8), 3210-3220.

- Caldwell, M. M., White, R. S., Moore, R. T., & Camp, L. B. (1977). Carbon balance, productivity, and water use of cold-winter desert shrub communities dominated by C₃ and C₄ species. *Oecologia*, 29(4), 275-300.
- Carey, J. C., Tang, J., Templer, P. H., Kroeger, K. D., Crowther, T. W., Burton, A. J., ... & Jiang, L. (2016). Temperature response of soil respiration largely unaltered with experimental warming. *Proceedings of the National Academy of Sciences*, 113(48), 13797-13802.
- Caves, J. K., Moragne, D. Y., Ibarra, D. E., Bayshashov, B. U., Gao, Y., Jones, M. M., ... & Chamberlain, C. P. (2016). The Neogene de-greening of Central Asia. *Geology*, 44(11), 887-890.
- Caves-Rugenstein, J. K. C., & Chamberlain, C. P. (2018). The evolution of hydroclimate in Asia over the Cenozoic: A stable-isotope perspective. *Earth-Science Reviews* 185, 1129-1156.
- Cerling, T. E. (1984). The stable isotopic composition of modern soil carbonate and its relationship to climate. *Earth and Planetary science letters*, 71(2), 229-240.
- Cerling, T. E. (1991). Carbon dioxide in the atmosphere: evidence from Cenozoic and Mesozoic paleosols. *American Journal of Science*, 291(4)
- Cerling, T. E. (1992). Use of carbon isotopes in paleosols as an indicator of the P (CO₂) of the paleoatmosphere. *Global Biogeochemical Cycles*, 6(3), 307-314.
- Cerling, T. E. (1999). Stable carbon isotopes in palaeosol carbonates. *Palaeoweathering, palaeosurfaces and related continental deposits*, 43-60.
- Cerling, T. E., & Quade, J. (1993). Stable carbon and oxygen isotopes in soil carbonates. *Climate change in continental isotopic records*, 78, 217-231.
- Cotton, J. M., & Sheldon, N. D. (2012). New constraints on using paleosols to reconstruct atmospheric p CO₂. *Bulletin*, 124(9-10), 1411-1423.
- Cotton, J. M., Sheldon, N. D., Hren, M. T., & Gallagher, T. M. (2015). Positive feedback drives carbon release from soils to atmosphere during Paleocene/Eocene warming. *American Journal of Science*, 315(4), 337-361.
- Craine, J. M., Wedin, D. A., & Chapin, F. S. (1999). Predominance of ecophysiological controls on soil CO₂ flux in a Minnesota grassland. *Plant and Soil*, 207(1), 77-86.

- Dai, S., Fang, X., Dupont-Nivet, G., Song, C., Gao, J., Krijgsman, W., ... & Zhang, W., 2006, Magnetostratigraphy of Cenozoic sediments from the Xining Basin: Tectonic implications for the northeastern Tibetan Plateau. *Journal of Geophysical Research: Solid Earth*, 111(B11).
- De Jong, E. (1981). Soil aeration as affected by slope position and vegetative cover. *Soil Science*, 131(1), 34-43.
- Dupont-Nivet, G., Krijgsman, W., Langereis, C. G., Abels, H. A., Dai, S., & Fang, X., 2007, Tibetan plateau aridification linked to global cooling at the Eocene–Oligocene transition. *Nature*, 445(7128), 635-638.
- Ekart, D. D., Cerling, T. E., Montanez, I. P., & Tabor, N. J. (1999). A 400 million year carbon isotope record of pedogenic carbonate: implications for paleoatmospheric carbon dioxide. *American Journal of Science*, 299(10), 805-827.
- Fan, M., Ayyash, S. A., Tripathi, A., Passey, B. H., & Griffith, E. M. (2018). Terrestrial cooling and changes in hydroclimate in the continental interior of the United States across the Eocene-Oligocene boundary. *GSA Bulletin*, 130(7-8), 1072-1084.
- Fang, X., Fang, Y., Zan, J., Zhang, W., Song, C., Appel, E., ... & Zhang, T. (2019). Cenozoic magnetostratigraphy of the Xining Basin, NE Tibetan Plateau, and its constraints on paleontological, sedimentological and tectonomorphological evolution. *Earth-Science Reviews*, 190, 460-485.
- Foster, G. (2019). A Cenozoic CO₂ Record from Marine Proxies, Version March 2019 <http://www.p-co2.org/>
- Foster, G. L., Royer, D. L., & Lunt, D. J. (2017). Future climate forcing potentially without precedent in the last 420 million years. *Nature Communications*, 8, 14845.
- Fouseki, E., & Margaris, N. S. (1981). Soil metabolism and decomposition in a phryganic (East Mediterranean) ecosystem. *Oecologia*, 50(3), 417-421.
- Gulbranson, E. L., Tabor, N. J., & Montañez, I. P. (2011). A pedogenic goethite record of soil CO₂ variations as a response to soil moisture content. *Geochimica et Cosmochimica Acta*, 75(22), 7099-7116.

Herzschuh, U., 2007. Reliability of pollen ratios for environmental reconstructions on the Tibetan Plateau. *Journal of Biogeography*, 34, 1265–1273.

Hoorn, C., Straathof, J., Abels, H. A., Xu, Y., Utescher, T., & Dupont-Nivet, G. (2012). A late Eocene palynological record of climate change and Tibetan Plateau uplift (Xining Basin, China). *Palaeogeography, Palaeoclimatology, Palaeoecology*, 344, 16-38.

Hough, B. G., Fan, M., & Passey, B. H. (2014). Calibration of the clumped isotope geothermometer in soil carbonate in Wyoming and Nebraska, USA: Implications for paleoelevation and paleoclimate reconstruction. *Earth and Planetary Science Letters*, 391, 110-120.

Hough, B. G., Garzzone, C. N., Wang, Z., Lease, R. O., Burbank, D. W., & Yuan, D. (2011). Stable isotope evidence for topographic growth and basin segmentation: Implications for the evolution of the NE Tibetan Plateau. *GSA Bulletin*, 123(1-2), 168-185.

Hudgens, D. E., & Yavitt, J. B. (1997). Land-use effect on soil methane and carbon dioxide fluxes in forests near Ithaca, New York. *Ecocence*, 4(2), 214-222.

Jia, Y., Wu, H., Zhu, S., Li, Q., Zhang, C., Yu, Y., & Sun, A. (2020). Cenozoic aridification in Northwest China evidenced by paleovegetation evolution. *Palaeogeography, Palaeoclimatology, Palaeoecology*, 109907.

Jian, J., Steele, M. K., Day, S. D., & Thomas, R. Q. (2018). Future global soil respiration rates will swell despite regional decreases in temperature sensitivity caused by rising temperature. *Earth's Future*, 6(11), 1539-1544.

Kim, S. T., & O'Neil, J. P. (1997). Equilibrium and nonequilibrium oxygen isotope effects in synthetic carbonates. *Geochimica et Cosmochimica Acta*, 61(16), 3461-3475.

Knapp, A. K., Conard, S. L., & Blair, J. M. (1998). Determinants of soil CO₂ flux from a sub-humid grassland: effect of fire and fire history. *Ecological Applications*, 8(3), 760-770.

Kohn, M. J. (2010). Carbon isotope compositions of terrestrial C₃ plants as indicators of (paleo) ecology and (paleo) climate. *Proceedings of the National Academy of Sciences*, 107(46), 19691-19695.

- Licht, A., Dupont-Nivet, G., Pullen, A., Kapp, P., Abels, H. A., Lai, Z., ... & Giesler, D. (2016). Resilience of the Asian atmospheric circulation shown by Paleogene dust provenance. *Nature communications*, 7, 12390.
- Licht, A., Van Cappelle, M., Abels, H. A., Ladant, J. B., Trabucho-Alexandre, J., France-Lanord, C., ... & Terry Jr, D., 2014, Asian monsoons in a late Eocene greenhouse world. *Nature*, 513(7519), 501-506.
- Liu, X., Sun, H., Miao, Y., Dong, B., & Yin, Z. Y. (2015). Impacts of uplift of northern Tibetan Plateau and formation of Asian inland deserts on regional climate and environment. *Quaternary Science Reviews*, 116, 1-14.
- Looy, C. V., Ranks, S. L., Chaney, D. S., Sanchez, S., Steyer, J. S., Smith, R. M., ... & Tabor, N. J. (2016). Biological and physical evidence for extreme seasonality in central Permian Pangea. *Palaeogeography, palaeoclimatology, palaeoecology*, 451, 210-226.
- Mahecha, M. D., Reichstein, M., Carvalhais, N., Lassus, G., Lange, H., Seneviratne, S. I., ... & Janssens, I. A. (2010). Global convergence in the temperature sensitivity of respiration at ecosystem level. *Science*, 329(5993), 838-840.
- Meijer, N., Dupont-Nivet, G., Abels, H. A., Kaya, M. Y., Licht, A., Xiao, M., ... & Guo, Z. (2019). Central Asian moisture modulated by proto-Paratethys Sea incursions since the early Eocene. *Earth and Planetary Science Letters*, 510, 73-84.
- Miller, K. G., Wright, J. D., Kutz, M. E., Wade, B. S., Browning, J. V., Cramer, B. S., & Rosenthal, Y. 2009, Climate threshold at the Eocene-Oligocene transition: Antarctic ice sheet influence on ocean circulation. *The Late Eocene Earth: Hothouse, Icehouse, and Impacts*, GSA Special Paper 452, 169.
- Montanez, I. P. (2013). Modern soil system constraints on reconstructing deep-time atmospheric CO₂. *Geochimica et Cosmochimica Acta*, 101, 57-75.
- Myers, T. S., Tabor, N. J., Jacobs, L. L., & Mateus, O. (2012). Estimating soil CO_{2atm} using paleosol carbonates: implications for the relationship between primary productivity and faunal richness in ancient terrestrial ecosystems. *Paleobiology*, 38(4), 585-604.

- Myers, T. S., Tabor, N. J., Jacobs, L. L., & Bussert, R. (2016). Effects of Different Organic-Matter Sources On Estimates of Atmospheric and Soil CO_{2atm} Using Pedogenic Carbonate. *Journal of Sedimentary Research*, 86(7), 800-812.
- Pagani, M., Huber, M., Liu, Z., Bohaty, S. M., Henderiks, J., Sijp, W., ... & DeConto, R. M. (2011). The role of carbon dioxide during the onset of Antarctic glaciation. *science*, 334(6060), 1261-1264.
- Page, M., Licht, A., Dupont-Nivet, G., Meijer, N., Barbolini, N., Hoorn, C., ... & Mulch, A. (2019). Synchronous cooling and decline in monsoonal rainfall in northeastern Tibet during the fall into the Oligocene icehouse. *Geology* 47(3), 203-206.
- Peel, M. C., Finlayson, B. L., & McMahon, T. A. (2007). Updated world map of the Köppen-Geiger climate classification. *Hydrology and earth system sciences discussions*, 4(2), 439-473.
- Quade, J., & Roe, L. J. (1999). The stable-isotope composition of early ground-water cements from sandstone in paleoecological reconstruction. *Journal of Sedimentary Research*, 69(3), 667-674.
- Quade, J., Cerling, T. E., & Bowman, J. R. (1989). Systematic variations in the carbon and oxygen isotopic composition of pedogenic carbonate along elevation transects in the southern Great Basin, United States. *Geological Society of America Bulletin*, 101(4), 464-475.
- Quade, J., Eiler, J., Daeron, M. & Achyuthan, H. (2013). The clumped isotope geothermometer in soil and paleosol carbonate. *Geochimica et Cosmochimica Acta*, 105, 92-107.
- Raich, J. W., & Potter, C. S. (1995). Global patterns of carbon dioxide emissions from soils. *Global Biogeochemical Cycles*, 9(1), 23-36.
- Retallack, G. J. (2005). Pedogenic carbonate proxies for amount and seasonality of precipitation in paleosols. *Geology*, 33(4), 333-336.
- Retallack, G. J. (2009). Refining a pedogenic-carbonate CO₂ paleobarometer to quantify a middle Miocene greenhouse spike. *Palaeogeography, Palaeoclimatology, Palaeoecology*, 281(1-2), 57-65.

- Romanek, C. S., Grossman, E. L., & Morse, J. W. (1992). Carbon isotopic fractionation in synthetic aragonite and calcite: effects of temperature and precipitation rate. *Geochimica et cosmochimica acta*, 56(1), 419-430.
- Steinthorsdottir, M., Porter, A. S., Holohan, A., Kunzmann, L., Collinson, M., & McElwain, J. C. (2016). Fossil plant stomata indicate decreasing atmospheric CO₂ prior to the Eocene–Oligocene boundary. *Climate of the Past*, 12(2), 439-454.
- Song, B., Spicer, R. A., Zhang, K., Ji, J., Farnsworth, A., Hughes, A. C., ... & Shen, T. (2020). Qaidam Basin leaf fossils show northeastern Tibet was high, wet and cool in the early Oligocene. *Earth and Planetary Science Letters*, 537, 116175.
- Sorrel, P., Eymard, I., Leloup, P. H., Maheo, G., Olivier, N., Sterb, M., ... & Li, H. (2017). Wet tropical climate in SE Tibet during the Late Eocene. *Scientific reports*, 7(1), 1-11.
- Tipple, B. J., Meyers, S. R., & Pagani, M. (2010). Carbon isotope ratio of Cenozoic CO₂: A comparative evaluation of available geochemical proxies. *Paleoceanography and Paleoclimatology*, 25(3).
- Tüfekçioğlu, A., Küçük, M., Bilmiş, T., Altun, L., & Yılmaz, M. (2010). Soil respiration and root biomass responses to burning in Calabrian pine (*Pinus brutia*) stands in Edirne, Turkey. *J. Environ. Biol.* 31, 15-19.
- Wang, Y., Cerling, T. E., & Effland, W. R. (1993). Stable isotope ratios of soil carbonate and soil organic matter as indicators of forest invasion of prairie near Ames, Iowa. *Oecologia*, 95(3), 365-369.
- Wu, J., Zhang, K., Xu, Y., Wang, G., Garzzone, C. N., Eiler, J., ... & Mahéo, G. (2018). Paleoelevations in the Jianchuan Basin of the southeastern Tibetan Plateau based on stable isotope and pollen grain analyses. *Palaeogeography, Palaeoclimatology, Palaeoecology*, 510, 93-108.
- Zhang, X., Nakawo, M., Yao, T., Han, J., & Xie, Z. (2002). Variations of stable isotopic compositions in precipitation on the Tibetan Plateau and its adjacent regions. *Science in China Series D: Earth Sciences*, 45(6), 481-493.
- Zhao, Z., Peng, C., Yang, Q., Meng, F. R., Song, X., Chen, S., ... & Zhu, Q. (2017). Model prediction of biome-specific global soil respiration from 1960 to 2012. *Earth's Future*, 5(7), 715-729.

Zheng, H., Wei, X., Tada, R., Clift, P. D., Wang, B., Jourdan, F., ... & He, M. (2015). Late oligocene–early miocene birth of the Taklimakan Desert. *Proceedings of the National Academy of Sciences*, 112(25), 7662-7667.

Journal Pre-proof

Biome	Measured annual soil respiration rate S (in gC/m ² /yr)										Measured summer soil respiration rate S (in gC/m ² /yr)						
	n (sites)	Mean	1σ	min	max	Q1	Q2 (median)	Q3	n (sites)	Mean	1σ	min	max	Q1	Q2 (median)	Q3	
Arctic	Desert/steppe/Tundra	40	247	207	1	663	61	186	364	5	444	177	212	666	367	405	566
	Grassland/shrubland	83	485	381	9	2198	169	455	646	19	966	1030	5	3030	203	534	1191
Boreal	Forest	280	599	450	27	3900	338	495	684	63	1124	847	0	3938	511	932	1447
	wetlands	70	279	173	7	930	153	238	371	7	1104	1206	246	3336	297	327	1613
Temperate	Desert	46	266	249	32	1190	102	189	324	0	-	-	-	-	-	-	-
	Grassland/shrubland	761	899	618	32	4330	407	730	1135	31	846	629	214	2840	450	648	1047
	Forest	1933	817	711	3	23046	534	735	980	73	946	831	0	2651	239	641	1434
	wetlands	0	608	414	64	1794	351	490	794	0	-	-	-	-	-	-	-
Mediterranean	Grassland/shrubland	104	684	412	15	1725	367	618	955	30	4038	3275	38	11171	1516	3512	6067
	Forest	187	860	446	27	7051	448	808	1097	27	933	548	246	2321	625	795	1111
Subtropical	Grassland/shrubland	31	974	491	219	2141	510	1055	1200	3	2072	857	1530	3060	1578	1626	2343
	Forest	544	934	476	55	6328	614	903	1163	4	226	79	170	337	170	199	255
Tropical	Grassland/shrubland	86	1312	861	107	4390	691	1039	1741	7	1117	1022	341	3060	388	489	1578
	Forest	517	1351	897	114	8136	891	1274	1679	6	1628	804	693	2874	1054	1570	2026

Table 1. Annual and summer soil respiration (R_s) for terrestrial biomes. Average, standard deviation, median and quartiles are calculated from the Soil Respiration Database (SRDB) Version 4.1 (Bond-Lamberty and Thomson, 2018), excluding cultivated sites.

Model parameters		
Depth of soil profile	z_p (in cm)	100 ± 20
Characteristic soil depth of CO ₂ production	z_c (in cm)	25 ± 10
Sampling depth in soil	z_s (in cm)	50 ± 10
Porosity	ε	0.6
Diffusional constant for CO ₂ in soil	D_s (in cm ² /s)	0.042
Carbon isotopic composition of the atmospheric CO ₂	$\delta^{13}C_{atm}$ (in ‰)	modern: -6.5
		Paleogene data: -6 ± 0.25
Age of the paleosol	Age (in kyr or Myr)	Modern: 0
		Paleogene: Estimated age by magnetostratigraphy and cyclostratigraphy ± 80 kyr
Carbonate growth temperature	T (in °C)	Modern: literature (see Supplementary Table 3)
		Paleogene: moving average across Xining clumped isotope temperatures of Page et al., (2019) (time windows: 2.4 Myr); uncertainty corresponds to the maximum standard deviation observed over the time window (from 3 to 7°C)
Atmospheric CO ₂ concentration	CO _{2atm} (in ppmV)	Modern: 400
		Paleogene: two sets: (a) moving average (time windows: 3.6 Myr) across a database of existing pCO ₂ values excluding data coming from soil paleobarometry (Beerling and Joyce, 2011; Zhang et al. 2013; Steinhorsdottir et al., 2016); error corresponds to quartiles Q1 and Q3 in the time window; (b) synthetic one-step pCO ₂ evolution with 800 ± 200 ppmV before 33.9 Ma, 400 ± 200 ppmV after 33.9 Ma.

Table 2. Model parameters for the soil respiration reconstructions. The table displays values for Monte Carlo parameters and their uniformly-distributed uncertainty, used for both modern soils (Table 3) and paleosols.

Biome	Boreal grassland			Temperate Desert			Temperate grassland				Temperate forest	Mediterranean grassland/shrubland				
Median, Q1 & Q3 soil respiration rate for the biome (in gC/m ² /yr)	191 (91-495)			203 (98 - 352)			730 (367 - 1032)				730 (510 - 964)	641 (342 - 910)				
Location	Saskatchewan			Utah			Minnesota	Kansas		New York		Provence	Turkey		Greece	
Approx respiration rate at nearby site (in gC/m ² /yr)	230			184-187			624-768		144-215		189-681		480-580		418-515	345-401
Source paper for respiration rate	de Jong (1981)			Caldwell et al (1977)			Craine et al (1999)		Knapp et al (1998)		Judgens and Lavitt (1997)		Billes et al (1971)		Tufekcioglu et al (2010)	Fouseki and Margaris (1981)
$\delta^{13}\text{C}_{\text{resp}}$ (in ‰)	24.2	24.1	22.1	24.5	24.4	23.8	17.8	20.7	15.7	14.0	-25.6	-25	24.5	24.5	-25.7	
$\delta^{13}\text{C}_{\text{carb}}$ (in ‰)	-7.9	-8.4	-6.3	-7.4	-7.5	-8.8	-1.9	-5.4	1.6	-0.4	-9.4	-10	-10	10.3	-9.3	
T (in °C)	20	20	20	23	23	23	21	21	26	26	21	17	27	27	23	
Source paper for isotopes and T	Cerling (1992). T = T _{growth} + 5°C			Cerling and Quade (1993). T = T _{max} at depth								Cerling (1992). T = T _{growth} + 5°C	Ekart et al (1999). T = T _{growth} + 5°C	Cerling and Quade (1993). T = T _{max} at depth		Cerling (1992). T = T _{growth} + 5°C
Modeled S(z) (in ppmV)	1168	1585	1250	746	796	1028	598	1378	1082	541	1297	3838	2600	2074	1084	
Modeled R _s (in gC/m ² /yr)	220 ± 43 (1σ)	299 ± 59 (1σ)	235 ± 46 (1σ)	140 ± 27 (1σ)	150 ± 29 (1σ)	170 ± 77 (1σ)	113 ± 22 (1σ)	260 ± 51 (1σ)	201 ± 39 (1σ)	100 ± 20 (1σ)	245 ± 49 (1σ)	736 ± 145 (1σ)	382 ± 75 (1σ)	478 ± 94 (1σ)	204 ± 40 (1σ)	

Table 3. Median soil and measured soil respiration compared to modelled soil respiration for various sites of different biomes. Median soil respiration values are from Table 1; note that measured respiration do not come from the same sites as isotopic and temperature data as both types of data are currently unavailable at the same sites. The carbonate growth temperature used for the model is either the growth season temperature + 5°C (following Brecker et al., 2009), or the maximal temperature at 50 cm depth, when available (Cerling and Quade, 1993).

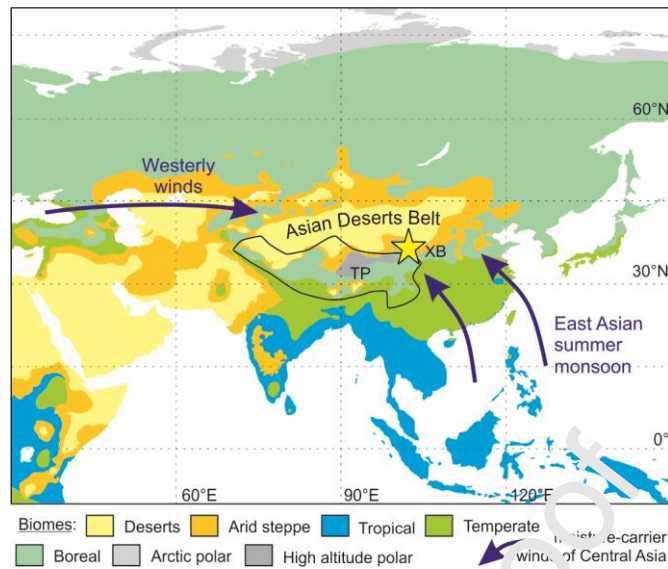


Fig. 1. Map of Asia and its different biomes (Peel et al., 2007), with location of the Xining Basin (XB) and Tibetan Plateau (TP, black line) and moisture-carrier wind directions feeding the Asian desert belts (blue arrows).

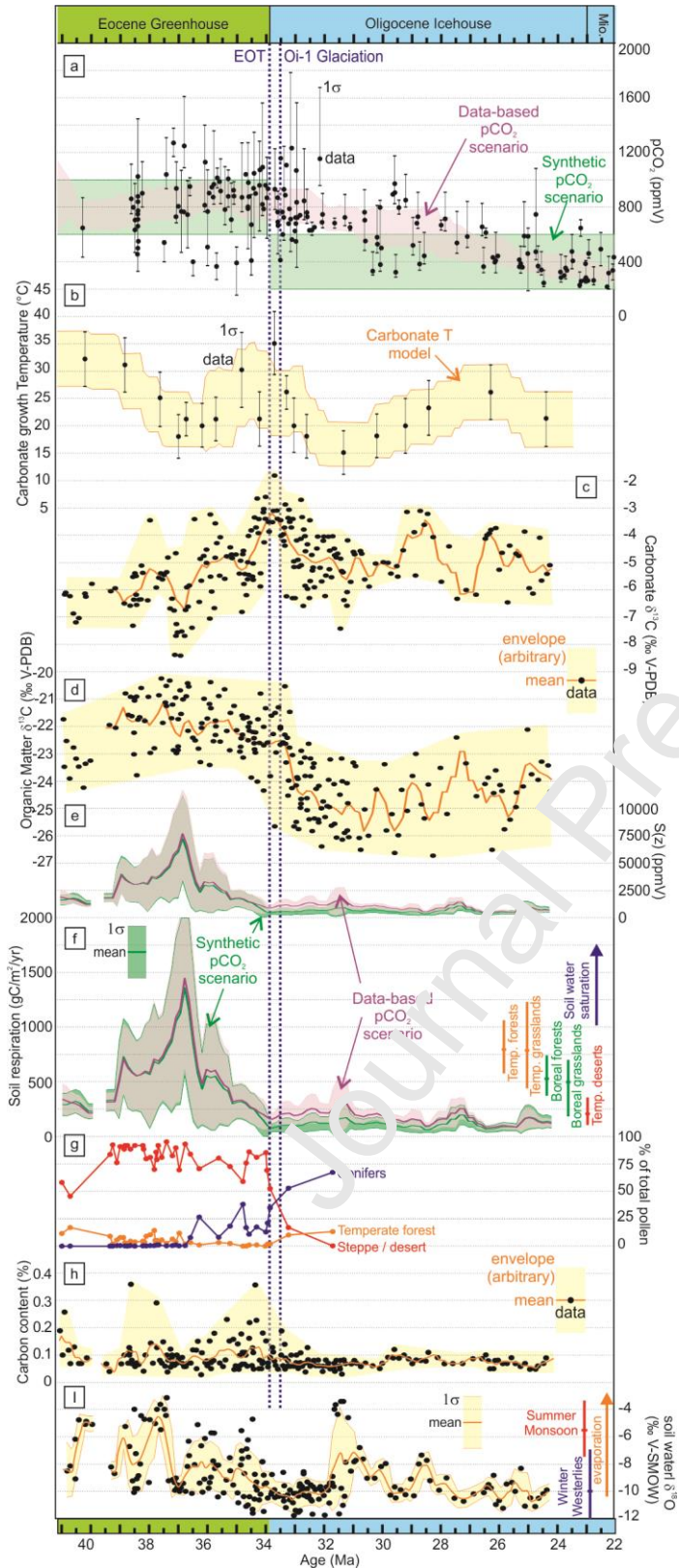


Fig. 2: CO_{2atm} evolution through the late Paleogene compared with soil carbonate growth temperature, soil carbon isotopic composition, reconstructed soil respiration R_s , pollen assemblages and soil water oxygen isotopic ratio in Xining. (a) Paleogene CO_{2atm} values (black dots with standard errors) and the two CO_{2atm} scenarios (shaded areas) used to reconstruct R_s . (b) Carbonate growth temperature derived from clumped isotopes (black dots with standard errors; Page et al., 2019); shaded area corresponds to the temperature model used to reconstruct R_s (moving average across the values); (c) Carbonate $\delta^{13}C$ and (d) organic matter $\delta^{13}C$ values (uncertainty < 0.01 ‰ V-PDB); (e) Reconstructed $S(z)$ and (f) soil respiration R_s in Xining for both CO_{2atm} scenarios (average and standard deviation); R_s is compared with soil respiration of temperate and boreal ecosystems ($Q1$, $Q3$ and median of Supplementary Table S1); blue arrow indicates the effect of soil water saturation on reconstructed R_s ; (g) Proportion in pollen assemblages of temperate forest, desert/steppe and conifer taxa in Xining sediment (Page et al., 2019); (h) Carbon content in

decarbonated sediment (in %); (i) Soil water oxygen isotopic ratios of carbonate samples ($1\sigma < 1$

‰, not shown) compared to seasonal rainfall isotopic composition in nearby Lanzhou city (Summer monsoon: May to Oct.; Winter westerlies: Nov. to Apr.; Araguas-Araguas et al., 1998); orange arrow indicates the effect of evaporation on soil water isotopic ratios.

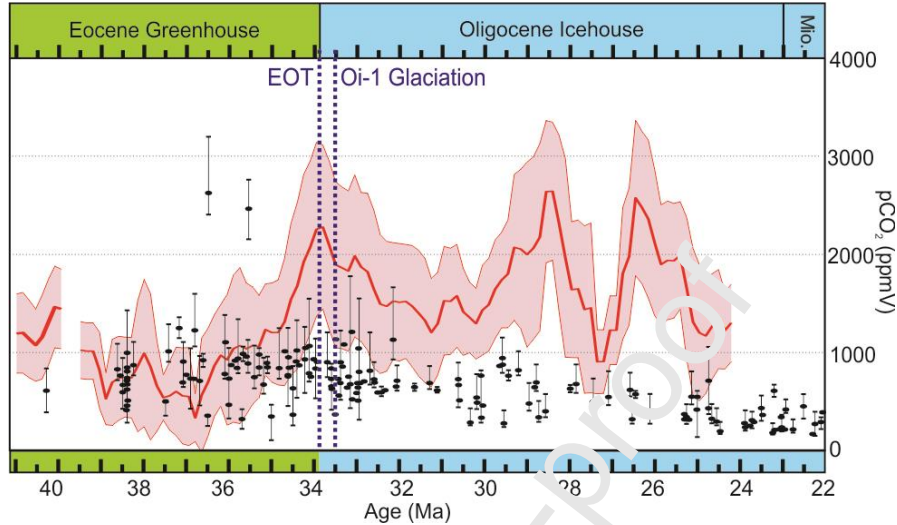


Fig. 3. Reconstructed CO_{2atm} using the standard soil paleobarometry approach. The CO_{2atm} values are reconstructed using R_s values of $+00 \pm 130 \text{ gC/m}^2/\text{yr}$ (see text). Reconstructed CO_{2atm} values are close to CO_{2atm} data from marine proxies (black dots with error bars) during the 38-36 Ma window but climb above 1000 ppmV in the Oligocene, reaching values episodically up to 2500 ppmV, five times more than what is predicted by other proxies.

Highlights

- We reconstruct past soil respiration rates from paleosols in northeastern Tibet.
- Soil respiration dropped at least 4-fold during the transition into the Oligocene.
- Boreal desert-steppes of Central Asia date back to the Oligocene.